Certainty of pretreatment apparent diffusion coefficient in the characterization of thyroid gland pathologies

Tarek Abd-Alhamid[a], Ahmed G. Khafagy[a], Hesham Al Sersy[a], Anas Askora[a], Tahany M. Rabie[a], Mohamed S. Taha[a], Amal Ebrahim[b], Hoda M. El Sayed[c]

[a]Otorhinolaryngology Department, [b]Radiology Department, [c]Internal Medicine Department, Faculty of Medicine, Ain Shams University, Cairo, Egypt

Correspondence to Ahmed Gamal Khafagy, MD, 44 Batrawy street, Nasr city, Cairo, Egypt; Tel: +20 109 392 4416; e-mail: ahmedgamal_2489@yahoo.com

Received 27 January 2016
Accepted 4 May 2016

The Egyptian Journal of Otolaryngology
2017, 33:495–501

Introduction
One of the most recent techniques in imaging tumors is the diffusion-weighted MRI. It provides information regarding the metabolic, molecular, and pathophysiological aspects of tumors, especially thyroid gland cancer. Diffusion-weighted imaging (DWI) has also been proposed as a sensitive marker for monitoring treatment response in head and neck cancers. The biophysical mechanism of DWI is based on the translational motion of water molecules in tissues. The magnitude of this motion is characterized by its apparent diffusion coefficient (ADC) values.

Objective
The aim of the present study was to evaluate the certainty of ADC value in differentiating between benign and malignant thyroid lesions.

Materials and methods
Neck MRI with several sequences including DWI in the axial plane were carried out for 49 patients who presented with thyroid masses either benign or malignant. ADC maps were calculated by using the MRI machine software.

Results
A total of 49 patients (77.6%) were included in the present study. There were 11 men (22.4%) and 38 women patients (77.6%), with a mean age of 44.4 years. The lesions were benign in 31 cases (63.3%) and malignant in 18 cases (36.7%). The ADC values were significantly different ($P < 0.001$) between benign and malignant lesions.

Conclusion
ADC value is a promising noninvasive imaging tool that can be used for characterization and differentiation of thyroid nodules.

Keywords:
apparent diffusion coefficient, diffusion-weighted image, MRI, nodule, thyroid

Egypt J Otolaryngol 33:495–501

1012-5574

Introduction

A differential diagnosis of benign and malignant lesions of the thyroid gland is critical as it enables clinicians to implement appropriate management strategies for malignant lesions. Nodular thyroid could be detected on palpation in 4–7% of the population [1,2]. However, on sonographic examination, this percentage rises to 10–40%, whereas on autopsy, it has been found to be 50% [3,4]. The primary assessment of thyroid lesions was for a long time carried out by using ultrasonography [2,5,6]. However, it was found that, there was no single sonographic criterion that could accurately differentiate between benign and malignant thyroid masses [4,7]. In addition, using color Doppler sonography in predicting thyroid cancer has been known to give contradictory results. The scintigraphic assessment of thyroid nodules carries the hazards of radiation exposure [2]. Different studies have concluded that not all hot nodules are benign [8,7]. They found that the risk for cancer in cold nodules is four times more common than in hot ones [3,8]. Despite that, fine needle aspiration cytology (FNAC) is known to be effective in distinguishing between benign and malignant nodules [4,5,9,10], it is inconclusive in 15–20% of patients, and carries the risk for hemorrhage [2,4]. To date, conventional MR and computed tomography (CT) continue to be the main imaging modalities for evaluating thyroid cancer. When making the diagnosis, both modalities suffer from low sensitivity and accuracy because they rely on volumetric and morphological criteria [10,11]. Moreover, because both entities may present with similar imaging features, changes after the treatment can be difficult to separate from tumor recurrence. Many studies showed the potential of ^{18}F-fluoro-deoxy-glucose (^{18}F-FDG) PET alone [12,13] or in combination with CT PET/CT in evaluating thyroid gland cancer. However, lower spatial resolution and problems with discriminating

neoplastic processes from inflammation and tissue reaction make the interpretation of PET images confounding [14]. Due to the fact that ^{18}F-FDG uptake is not specific to cancer, false positive findings, owing to inflammatory processes and metabolically active regions, are also common in the thyroid region [15]. Recently, the high technology in MR techniques provided information regarding the metabolic, molecular, and pathophysiological aspects of a tumor. One of the techniques is the diffusion-weighted MRI (DW-MRI) [16,17]. It can be used in the initial diagnostic characterization of thyroid gland cancer. Diffusion-weighted imaging (DWI) has also been proposed as a sensitive marker for monitoring treatment response in head and neck cancers [18]. The biophysical mechanism of DWI is based on the microscopic random translational motion of water molecules in biological tissues. The magnitude of this motion is characterized by its apparent diffusion coefficient (ADC) values. Variation in ADC values reflects the alteration and redistribution of water molecules between intracellular and extracellular compartments of a tissue [19]. Wang *et al.* [20] reported that the mean ADC value of benign solid lesions was significantly higher than that of malignant tumors. Tezuka *et al.* [21] showed in their study that DW-MRI could be clinically important in evaluating the thyroid function. Many researchers have concluded that ADC maps help in selecting the best biopsy site and in detecting tumor viability in post-treatment follow-up after radiation therapy [22–25]. The aim of the present study was to evaluate the certainty of ADC values in differentiating between benign and malignant thyroid lesions.

Materials and methods

The present study was carried out with the approval of the Institutional Review Board and the Ethical Committee of Ain University Hospitals. All participants provided an informed written consent. This prospective study was carried out between March 2013 and July 2015.

Inclusion criteria and exclusion criteria

Patients presented to the otorhinolaryngology outpatient clinic with goitre were evaluated. Complete history and physical examination focusing on the thyroid gland and adjacent cervical lymph nodes were carried out. The clinical assessment of thyroid nodules included the assessment of local symptoms (e.g. hoarseness), symptoms of thyroid dysfunction, medical history of thyroid problems/intervention, and family history of thyroid problems. A history of head and neck irradiation was especially important, as this increases the risk for thyroid cancer. Patients with (a) diffuse goitre, (b) previous history of thyroid surgery, (c) who had undergone neck irradiation, or (d) patients with contraindications to MRI, such as patients with a heart pacemaker, a metallic foreign body (metal sliver) in their eye, who have an aneurysm clip in their brain, or metallic devices placed in their cervical spines were excluded from the study. Neck ultrasonography was performed as a part of the evaluation of the goitre. Only patients with nodular goitre were enrolled and were subjected to FNAC and/or thyroid surgery if indicated according to the revised American Thyroid Association Management guidelines for patients with thyroid nodules and differentiated thyroid cancer [26]. The radiologist was blinded to the preoperative staging for malignant lesions and histopathology reports until the end of the study.

MRI

MRI was performed for all patients by using a 1.5-T MR [Achieva; Philips Medical Systems, the Netherlands (B. V.)]. A neck circular surface coil was used. The magnet was equipped with a self-shielded gradient set for echo-planar imaging. Patients were positioned in the supine position and were informed to avoid movement and swallowing during the examination. Scout scans were taken in the axial, coronal, and sagittal planes. After localizing the lesion, several sequences were taken, including the following:

(1) Axial T1-weighted fast spin echo images with the following parameters: repetition time (TR) in ms/ echo time (TE) in ms of 550/20, slice thickness of 4 mm, intersection gap of 1 mm, FOV of 210–230, matrix of 300 × 264 pixel, and a flip angle of 90°.
(2) Axial T2-weighted fast spin echo images with TR/ TE of 3973/80, slice thickness of 4 mm, intersection gap of 1 mm, FOV of 210–230, matrix of 232 × 198 pixel, and a flip angle of 90°.
(3) Sagittal T2-weighted fast spin echo images with TR/TE of 3500/100, slice thickness of 4 mm, intersection gap of 1 mm, FOV of 250–250, matrix of 300 × 264 pixel, and a flip angle of 90°.
(4) Coronal short tau inversion recovery with TR/TE/ TI of 2200/60/180 ms, slice thickness of 4 mm, intersection gap of 1 mm, FOV of 200–215, matrix of 200 × 154 pixel, and a flip angle of 90°.
(5) DWI were obtained in the axial plane. Imaging parameters were as follows: TR/TE of 2500 ms/ 100 ms, slice thickness of 4 mm, intersection gap of 1 mm, FOV of 250–250 mm, matrix of 124 × 124, NEX 4, and a bandwidth of 1617.5 kHz. The diffusion gradients were applied in three orthogonal directions (X, Y, and Z). The images

were acquired using *b*-values (0, 250, and 500 s/mm^2) with an average scan time of 34 s.
(6) ADC maps were automatically calculated by the MRI machine software and included in the sequence.

Fat suppression was added to the DWI by placing the frequency-selective radiofrequency pulse before the pulse sequence to avoid severe chemical-shift artifacts.

Calculation of apparent diffusion coefficient value

For quantitative analysis of tissue-specific diffusion capacities, the ADC was calculated according to the following equation: 22: ADC=log (SI1/SI2)/($b_2 - b_1$), where SI1 and SI2 are the signal intensities (SI) of DWIs, which can be obtained with two different *b*-values (b_1=0 s/mm^2 and b_{2max}, respectively) in the user-defined regions of interest.

Statistical methods

Statistical analysis was carried out using the MedCalc© version 14 (MedCalc© Software bvba; Ostend, Belgium). The Shapiro–Wilk test was used to examine the normality of the numerical data distribution. Normally distributed numerical data were presented as mean ± SD and skewed data as median (interquartile). Categorical data were presented as ratio or number (%). The independent-samples *t*-test was used to compare the intergroup differences as regards normally distributed numerical data. For comparison of skewed numerical data, the Mann–Whitney test was used. Fisher's exact test was used to compare independent categorical data. Receiver-operating characteristic (ROC) curve analysis was used to examine the value of the ADC for discrimination between benign or malignant lesions. All *P*-values were two-tailed. A *P*-value of less than 0.05 was considered statistically significant.

Results

Three patients were excluded from the study due to motion artifacts in two patients and bad image quality in another.

Demographic data and clinical characteristics of the patients

A total of 49 patients were included in this study. Of them, 11 (22.4%) were men and 38 (77.6%) were women. Their mean age was 44.4 ± 10.6 years (ranging from 20 to 65 years). The final histopathology of the thyroid gland lesions was benign in 31 cases (63.3%) and malignant in 18 cases (36.7%). The histological diagnoses of the benign lesions were follicular adenoma (n=8) and multinodular goitre (n=23). The histological diagnoses of malignant tumors were papillary carcinoma (n=11), follicular carcinoma (n=4), medullary carcinoma (n=2), and anaplastic carcinoma (n=1) (Table 1). There was no significant difference regarding age and sex between patients with benign nodules and those with malignant ones. The median ADC value of all cases was 1.4 and the interquartile range was 0.88–1.73 (Table 1). The median ADC value for benign lesions was 1.6 and the interquartile range was 1.5–1.9 (Fig. 1). The median ADC value for malignant lesion was 0.7 and the range was 0.6–0.9 (Fig. 2).

We found insignificant differences in the median ADC values of the various benign nodules. In addition, there were insignificant differences in the median ADC values of the various malignant nodules (Fig. 3). The ADC values were significantly different ($P<0.001$) between benign and malignant lesions (Table 2). Using the ROC curve analysis, an ADC value of less than or equal to 1×10^{-3} mm^2/s was found to be a plausible cutoff point to differentiate benign from malignant lesions (Fig. 4).

The diagnostic performance of DW-MRI for the identification of malignant lesions showed that the sensitivity, specificity, positive predictive value, and negative predictive value were 100, 100, 100, and 100%, respectively.

Discussion

Recently, thyroid imaging has markedly progressed, facilitating the evaluation and follow-up of thyroid masses [27]. DWI plays an important role in differentiating benign from malignant nodules of the thyroid gland. Reduced ADC values have been reported for most malignant tumors [28]. The diffusion technique produces different contrasts in different kinds of tissue. Therefore, the findings of

Table 1 Characteristics of the whole study population

Variable	Value
Age (years)	44.4 ± 10.6
Male/female	11/38
Histopathological type	
Follicular adenoma	8 (16.3%)
MNG	23 (46.9%)
Papillary carcinoma	11 (22.4%)
Follicular carcinoma	4 (8.2%)
Medullary carcinoma	2 (4.1%)
Anaplstic carcinoma	1 (2.0%)
Nature of lesion	
Benign	31 (63.3%)
Malignant	18 (36.7%)
ADC value (×10^{-3} mm^2/s)	1.4 (0.88 to 1.73)

Data are presented as mean ± SD, ratio, number (%), or median (interquartile range).

Figure 1

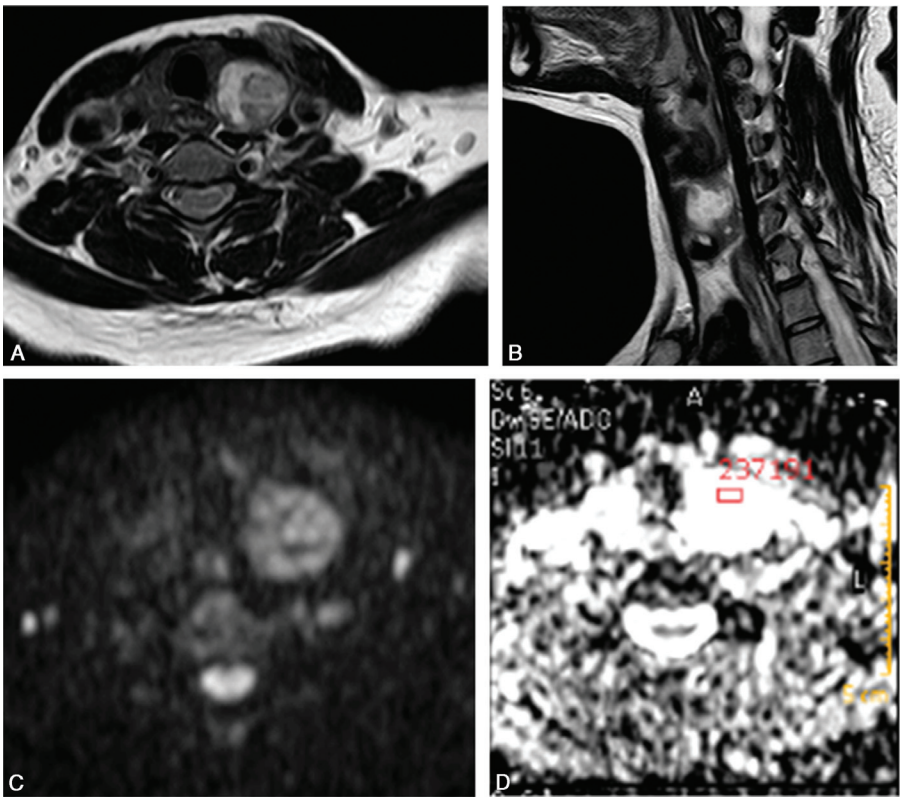

Follicular adenoma. (a) Axial T2-WI. The left thyroid lobe shows a large nodule hyperintense on T2-WI with internal areas of low signal (b) coronal T2-WI shows calcified nodule. (c) Diffusion-weighted images (DWI) (d) apparent diffusion coefficient (ADC) value between 1.6×10^{-3} mm^2/s suggesting benign nature.

Figure 2

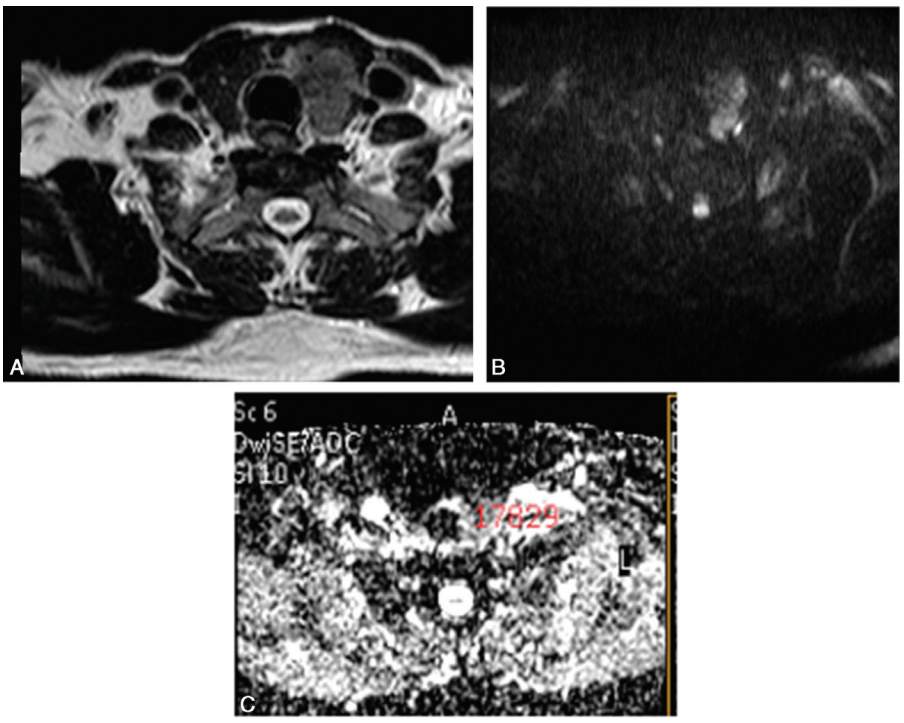

Papillary carcinoma. (a) The left thyroid lobe shows a large nodule 3×2.7 cm of intermediate signal on T2-WI. (b) Diffusion images. (c) Apparent diffusion coefficient (ADC) value 0.8×10^{-3} mm^2/s in keeping with the malignant nature.

Figure 3

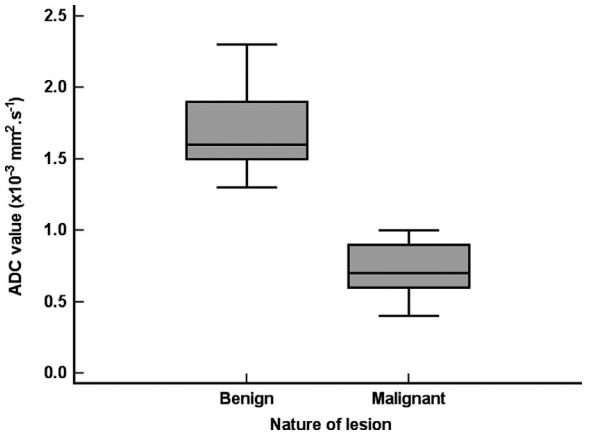

Box plot showing the apparent diffusion coefficient (ADC) value associated with benign or malignant lesions.

Figure 4

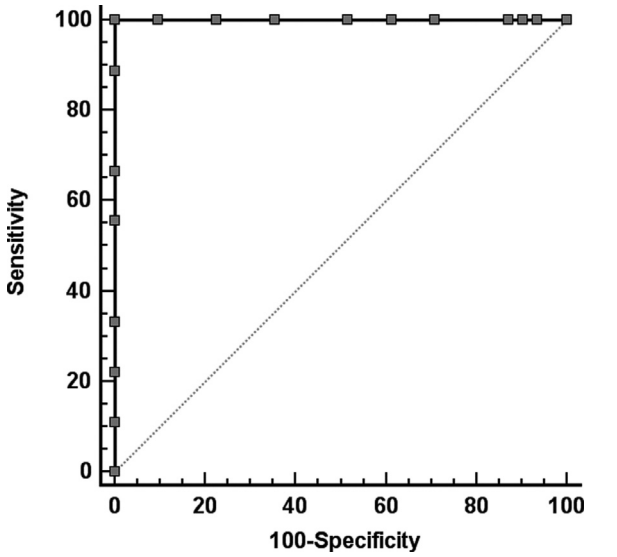

Receiver-operating characteristic (ROC) curve for the differentiating between benign or malignant lesions using the apparent diffusion coefficient (ADC) value.

Table 2 Characteristics of patients with benign or malignant lesions

Variable	Benign (n = 31)	Malignant (n = 18)	p-value
Age (years)	43.2 ± 11.2	46.5 ± 9.5	0.302[¶]
Male/female	7/24	4/14	1.000[§]
ADC value ($\times 10^{-3}$ mm^2/s)	1.6 (1.5 to 1.9)	0.7 (0.6 to 0.9)	<0.0001[¥]

Data are presented as mean ± SD, ratio, or median (interquartile range). [¶]Independent-samples *t* test. [§]Fisher's exact test. [¥]Mann-Whitney test.

this procedure can provide different information about diseased tissue [29]. By comparing differences in the ADC values between tissues, tissue characterization becomes possible [20] and can be used as a marker to distinguish malignant from benign head and neck lesions. Many recent studies reported that DWI has been used to differentiate benign and malignant head and neck masses, and to characterize cervical lymph nodes, salivary tumors, thyroid nodules, and sinonasal masses [30–35]. DWI has also been widely used for predicting and monitoring response to therapy [36–38].

In the present study, the median ADC value for malignant thyroid gland tumors was significantly lower ($P < 0.0001$) than that for benign lesions. We calculated an optimal ADC cutoff value of less than or equal to 1×10^{-3} mm^2/s, which was best used for differentiating benign from malignant lesions of the thyroid glands. In addition, as a result of ROC curve analysis, benign thyroid glands tumors could be differentiated from other malignant ones using this cutoff value with sensitivity, specificity, positive predictive value, and negative predictive value of 100, 100, 100, and 100%, respectively. This can be explained by the fact that a malignant lesion in thyroid glands is characterized by compact cellularity that leads to an increase in the nucleocytoplasmic ratio. These changes result in the reduction of extracellular space, which restricts diffusional motion of water protons, which in turn leads to ADC reduction [39]. Furthermore, reduced ADC values thought to be due to cellular membranes impede the mobility of water protons [28].

Comparable threshold ADC values have been reported in the literature for other head and neck lesions [30,40–42]. In accordance with our study, Razek and colleagues reported a significant difference in the ADC values for benign and malignant thyroid nodules. All benign nodules had higher mean ADC values (1.8×10^{-3} mm^2/s) compared with the malignant ones (0.73×10^{-3} mm^2/s). As a result of their ROC, the cutoff value to differentiate benign from malignant solitary thyroid nodules was 0.98×10^{-3} mm^2/s, with a sensitivity of 97.5%, a specificity of 91.7%, and an accuracy of 98.9%. Their explanation for high ADC values for benign nodules was the relative abundance of colloid follicles, microcystic necrosis, hemorrhage, and fibrous tissue. Calcified psammoma bodies in PTC and hyperplastic nuclei are responsible for low ADC values for malignant nodules [32]. Erdem *et al.* [28] also suggested that tiny calcification was closely correlated with the reduction of ADC values in thyroid malignancy. Delormere [43] demonstrated that malignant tumors usually do not have a complete basal membrane of blood vessel, which enhances the molecular exchange in the capillary bed. ADC values could be influenced by both extracellular space and blood perfusion. In thyroid

malignancy, increased blood perfusion increases the apparent speed of the diffusing water protons while the narrow extracellular space restricts its movement.

Recently, promising results have been reported regarding the use of DW-MRI and ADC in differentiating benign from malignant laryngeal lesions. Taha *et al.* [44,45] found that the ADC cutoff value was $1.1\times10^{-3}\,mm^2/s$, with a sensitivity, specificity, positive predictive value, and negative predictive value of 94, 100, 100, and 89%, respectively. They concluded that an ADC threshold of $1.1\times10^{-3}\,mm^2/s$ is optimal for distinguishing laryngeal carcinomas from benign lesions [43]. They also calculated an optimal ADC cutoff value of $1.3\times10^{-3}\,mm^2/s$, which was best used for differentiating benign from malignant lesions of the sinonasal tract. They stated that adding DW-MRI to conventional MRI increases the certainty in the tissue characterization of the sinonasal lesions. ADC mapping is an easy, promising tool for the characterization of sinonasal lesions [45].

On the other hand, there were other contradicting studies [46–48]. ADC values were predominantly higher for malignant thyroid nodules than those for benign ones, with values equal or more than $2.25\times10^{-3}\,mm^2/s$. They claimed that the higher ADC values may be due to the overproduction of thyroprotein follicles in malignant thyroid nodules, which do not restrict the diffusion of water protons. In their opinion, hemorrhage, microcystic necrosis, and calcification occur in both adenoma and carcinoma, causing restricted diffusion in adenoma as well as in carcinoma [49].

We could not differentiate between the different types of carcinoma on the basis of their specific ADC values. This was in agreement with Razek *et al.* [32]. They reported that it is not possible to differentiate the various thyroid gland carcinomas by their specific cell attenuation. In addition, Weidekamm *et al.* [46,47] showed in their study that the differentiation of the different types of carcinoma, such as papillary, medullary, and follicular thyroid carcinoma, is not possible with DWI, and suggested that blood tests enable accurate diagnosis of medullary carcinoma on the basis of elevated basal and pentagastrin-stimulated calcitonin levels, and follow-up of calcitonin levels in postoperative patients.

There were insignificant differences in the ADC values among various benign thyroid lesions in our study. However, in their study, Razek *et al.* [32] showed a significant difference in the ADC values between thyroid cysts and the solid nodules (adenomatous nodules and follicular adenomas), with a *P*-value of less than 0.0001. A thyroid cyst has the highest ADC value because it may contain serous fluid or may be a colloid cyst with high thyroglobulin concentration, whereas the solid nodule is formed of compact of crowded cells that may be attributed to low ADC values [32].

There still were some limitations of this study. The relatively small number (18 cases) of malignant nodules may limit the statistical power of the study. Multicenter studies with larger number of patients are needed to get better results. DW-MRI modality needs to be compared with other imaging modalities like PET/CT scan. Moreover, introduction of several innovative readout strategies will provide better-quality DWI images. Better image quality will improve the sensitivity and specificity of DWI in the characterization and differential diagnosis of head and neck cancers and ADC maps from the head and neck region [50].

Conclusion

The ADC value is a promising noninvasive imaging tool that can be used for characterization of thyroid nodules and differentiation between benign and malignant ones. We recommend that DW-MRI might be added to the routine imaging technique to differentiate malignant from benign thyroid nodules.

Financial support and sponsorship

Nil.

Conflicts of interest

There are no conflicts of interest.

References

1 Reading CC, Charboneau JW, Hay ID, Sebo TJ. Sonography of thyroid nodules: a 'classic pattern' diagnostic approach. Ultrasound Q 2005; 21:157–165.

2 Weber AL, Randolph G, Aksoy FG. The thyroid and parathyroid glands. CT and MR imaging and correlation with pathology and clinical findings. Radiol Clin North Am 2000; 38:1105–1129.

3 Tan GH, Gharib H, Reading CC. Solitary thyroid nodule. Comparison between palpation and ultrasonography. Arch Intern Med 1995; 155: 2418–2423.

4 Solbiati L, Osti V, Cova L, Tonolini M. Ultrasound of thyroid, parathyroid glands and neck lymph nodes. Eur Radiol 2001; 11:2411–2424.

5 Gooding G. Sonography of the thyroid and parathyroid. Radiol Clin North Am 1993; 31:967–989.

6 Bartolotta TV, Midiri M, Galia M, Runza G, Attard M, Savoia G, *et al.* Qualitative and quantitative evaluation of solitary thyroid nodules with contrast-enhanced ultrasound: initial results. Eur Radiol 2006; 16:2234–2241.

7 Yousem DM. Parathyroid and thyroid imaging. Neuroimaging Clin N Am 1996; 6:435–459.

8 Sahin M, Guvener N, Ozer F, *et al.* Thyroid cancer in hyperthyroidism: incidence rate and value of ultrasound-guided fine-needle aspiration biopsy in this patient group. J Endocrinol Invest 2005; 28:815–818.

9 Okamoto T, Yamashita T, Harasawa A. Test performance of three diagnostic procedures in evaluating thyroid nodules: physical examination,

ultrasonography and fine needle aspiration cytology. Endocr J 1994; 41: 243–247.

10 Altavilla G, Pascale M, Nenci I. Fine needle aspiration cytology of thyroid gland diseases. Acta Cytol 1990; 34:251–256.

11 Gharib H, Goellner JR. Fine-needle aspiration biopsy of the thyroid: an appraisal. Ann Intern Med 1993; 118:282–289.

12 Schechter NR, Gillenwater AM, Byers RM, Garden AS, Morrison WH, Nguyen LN, *et al.* Can positron emission tomography improve the quality of care for head-and-neck cancer patients?. Int J Radiat Oncol Biol Phys 2001; 51:4–9.

13 Schwartz DL, Rajendran J, Yueh B, Coltrera M, Anzai Y, Krohn K, Eary J. Staging of head and neck squamous cell cancer with extended-field FDG-PET. Arch Otolaryngol Head Neck Surg 2003; 129:1173–1178.

14 Yao M, Smith RB, Graham MM, Hoffman HT, Tan H, Funk GF, *et al.* The role of FDG PET in management of neck metastasis from head-and-neck cancer after definitive radiation treatment. Int J Radiat Oncol Biol Phys 2005; 63:991–999.

15 McCollum AD, Burrell SC, Haddad RI, *et al.* Positron emission tomography with 18F-fluorodeoxyglucose to predict pathologic response after induction chemotherapy and definitive chemoradiotherapy in head and neck cancer. Head Neck 2004; 26:890–896.

16 Mukherji SK, Schiro S, Castillo M, Kwock L, Muller KE, Blackstock W. Proton MR spectroscopy of squamous cell carcinoma of the extracranial head and neck: in vitro and in vivo studies. Am J Neuroradiol 1997; 18:1057–1072.

17 Star-Lack JM, Adalsteinsson E, Adam MF, *et al.* In vivo1h MR spectroscopy of human head and neck lymph node metastasis and comparison with oxygen tension measurements. Am J Neuroradiol 2000; 21:183–193.

18 Kim S, Loevner L, Quon H, Sherman E, Weinstein G, Kilger A, Poptani H. Diffusion-weighted magnetic resonance imaging for predicting and detecting early response to chemoradiation therapy of squamous cell carcinomas of the head and neck. Clin Cancer Res 2009; 15:986–994.

19 Padhani AR, Liu G, Koh DM, Chenevert TL, Thoeny HC, Takahara T, *et al.* Diffusion-weighted magnetic resonance imaging as a cancer biomarker: consensus and recommendations. Neoplasia 2009; 11:102–125.

20 Wang J, Takashima S, Takayama F, Kawakami S, Saito A, Matsushita T, *et al.* Head and neck lesions: characterization with diffusion-weighted echo-planar MR imaging. Radiology 2001; 220:621–630.

21 Tezuka M, Murata Y, Ishida R, Ohashi I, Hirata Y, Shibuya H. MR imaging of the thyroid: correlation between apparent diffusion coefficient and thyroid gland scintigraphy. J Magn Reson Imaging 2003; 17:163–169.

22 Lemaire L, Howe FA, Rodrigues LM, Griffiths JR. Assessment of induced rat mammary tumour response to chemotherapy using the apparent diffusion coefficient of tissue water as determined by diffusion-weighted 1H-NMR spectroscopy in vivo. MAGMA 1999; 8:20–26.

23 Mardor Y, Roth Y, Ochershvilli A, Spiegelmann R, Tichler T, Daniels D, *et al.* Pretreatment prediction of brain tumors' response to radiation therapy using high b-value diffusion-weighted MRI. Neoplasia 2004; 6:136–142.

24 Dzik-Jurasz A, Domenig C, George M, Wolber J, Padhani A, Brown G, Doran S. Diffusion MRI for prediction of response of rectal cancer to chemoradiation. Lancet 2002; 360:307–308.

25 McVeigh PZ, Syed AM, Milosevic M, Fyles A, Haider MA. Diffusion-weighted MRI in cervical cancer. Eur Radiol 2008; 18:1058–1064.

26 Cooper DS, Doherty GM, Haugen BR, Kloos RT, Lee SL, Mandel SJ, *et al.* American Thyroid Association (ATA) Guidelines Taskforce on Thyroid Nodules and Differentiated Thyroid Cancer Revised American Thyroid Association management guidelines for patients with thyroid nodules and differentiated thyroid cancer. Thyroid 2009; 19:1167–1214.

27 Soto GD, Halperin I, Squarcia M, Lomeña F, Domingo MP. Update in thyroid imaging. The expanding world of thyroid imaging and its translation to clinical practice. Hormones (Athens) 2010; 9:287–298.

28 Erdem G, Erdem T, Muammer H, Mutlu DY, Firat AK, Sahin I, Alkan A. Diffusion-weighted images differentiate benign from malignant thyroid nodules. J Magn Reson Imaging 2010; 31:94–100.

29 Koh DM, Padhani AR. Diffusion-weighted MRI: a new functional clinical technique for tumour imaging. Br J Radiol 2006; 79:633–635.

30 Ginat DT, Mangla R, Yeaney G, Johnson M, Ekholm S. Diffusion-weighted imaging for differentiating benign from malignant skull lesions and correlation with cell density. Am J Roentgenol 2012; 198:597–601.

31 Habermann CR, Arndt C, Graessner J, Diestel L, Petersen KU, Reitmeier F, *et al.* Diffusion-weighted echo-planar MR imaging of primary parotid gland tumors: is a prediction of different histologic subtypes possible?. Am J Neuroradiol 2009; 30:591–596.

32 Razek AA, Sadek AG, Kombar OR, Elmahdy TE, Nada N. Role of apparent diffusion coefficient values in differentiation between malignant and benign solitary thyroid nodules. Am J Neuroradiol 2008; 29:563–568.

33 Razek AA, Gaballa G, Elhawarey G, *et al.* Characterization of pediatric head and neck masses with diffusion-weighted MR imaging. Eur Radiol 2009; 19:201–208.

34 White ML, Zhang Y, Robinson RA. Evaluating tumors and tumor like lesions of the nasal cavity, the paranasal sinuses, and the adjacent skull base with diffusion-weighted MRI. J Comput Assist Tomogr 2006; 30:490–495.

35 Anderson JR, Tumors I. General features, types and examples. In: Levison DA, Reid R, Burt AD, Harrison DJ, Fleming S, eds. Muir's textbook of pathology 14th edLondon: Hodder Arnold Publication; 2008;127–156.

36 Thoeny HC, De Keyzer F, Chen F, Ni Y, Landuyt W, Verbeken EK, *et al.* Diffusion-weighted MR imaging in monitoring the effect of a vascular targeting agent on rhabdomyosarcoma in rats. Radiology 2005; 234:756–764.

37 Byun WM, Shin SO, Chang Y, Lee SJ, Finsterbusch J, Frahm J. Diffusion-weighted MR imaging of metastatic disease of the spine: assessment of response to therapy. Am J Neuroradiol 2002; 23:906–912.

38 Chen CY, Li CW, Kuo YT, *et al.* Early response of hepatocellular carcinoma to trans catheter arterial chemoembolization: choline levels and MR diffusion constants–initial experience. Radiology 2006; 239:448–456.

39 MacSween RNM, Whaley K. Muir's textbook of pathology. 13th ed. London Hodder & Stoughton 1992.

40 Sumi M, Nakamura T. Diagnostic importance of focal defects in the apparent diffusion coefficient-based differentiation between lymphoma and squamous cell carcinoma nodes in the neck. Eur Radiol 2009; 19:975–981.

41 Razek AA, Megahed AS, Denewer A, Motamed A, Tawfik A, Nada N. Role of diffusion-weighted magnetic resonance imaging in differentiation between the viable and necrotic parts of head and neck tumors. Acta Radiol 2008; 49:364–370.

42 Abdel Razek A, Mossad A, Ghonim M. Role of diffusion-weighted MR imaging in assessing malignant versus benign skull-base lesions. Radiol Med 2011; 116:125–132.

43 Delorme S, Knopp MV. Non-invasive vascular imaging: assessing tumour vascularity. Eur Radiol 1998; 8:517–527.

44 Taha MS, Amir M, Hassan O, Sabra R, Taha T, Riad MA. Pre-treatment apparent diffusion coefficient mapping: differentiation of benign from malignant laryngeal lesions. J Laryngol Otol 2015; 129:57–62.

45 Taha MS, El Fiky LM, Taha TM, Sabra RM, Youssef TA, Nada IM. Utility of apparent diffusion coefficient in characterization of different sinonasal pathologies. Am J Rhinol Allergy 2014; 28:181–186.

46 Schueller-Weidekamm C, Kaserer K, Schueller G, Scheuba C, Ringl H, Weber M, *et al.* Can quantitative diffusion-weighted MR imaging differentiate benign and malignant cold thyroid nodules? Initial results in 25 patients. Am J Neuroradiol 2009; 30:417–422.

47 Schueller-Weidekamm C, Schueller G, Kaserer K, Scheuba C, Ringl H, Weber M, *et al.* Diagnostic value of sonography, ultrasound-guided fine-needle aspiration cytology, and diffusion-weighted MRI in the characterization of cold thyroid nodules. Eur J Radiol 2010; 73:538–544.

48 Wu Y, Yue X, Shen W, Du Y, Yuan Y, Tao X, Tang CY. Diagnostic value of diffusion-weighted MR imaging in thyroid disease: application in differentiating benign from malignant disease. BMC Med Imaging 2013; 13:23.

49 Katz JF, Kane RA, Reyes J, Clarke MP, Hill TC. Thyroid nodules: sonographic-pathologic correlation. Radiology 1984; 151:741–745.

50 Chawla S, Kim S, Wang S, Poptani H. Diffusion-weighted imaging in head and neck cancers. Future Oncol 2009; 5:959–975.